# Diapycnal diffusivity at the upper boundary of the tropical North Atlantic oxygen minimum zone

Donata Banyte,[1] Toste Tanhua,[1] Martin Visbeck,[1] Douglas W. R. Wallace,[2] Johannes Karstensen,[1] Gerd Krahmann,[1] Anke Schneider,[1] Lothar Stramma,[1] and Marcus Dengler[1]

Received 18 November 2011; revised 19 July 2012; accepted 24 July 2012; published 14 September 2012.

[1] A deliberate tracer release experiment in 2008–2010 was used to study diapycnal mixing in the tropical northeastern Atlantic. The tracer ($CF_3SF_5$) was injected on the isopycnal surface $\sigma_\Theta = 26.88$ kg m$^{-3}$, which corresponds to about 330 m depth. Three surveys, performed 7, 20, and 30 months after the release, sampled the vertically and laterally expanding tracer patch. The mean diapycnal mixing estimate over the entire region occupied by the tracer and the period of 30 months was found to be $(1.19 \pm 0.18) \times 10^{-5}$ m$^2$ s$^{-1}$, or, alternatively, $(3.07 \pm 0.58) \times 10^{-11}$ (kg m$^{-3}$)$^2$ s$^{-1}$ as computed from the advection-diffusion equation in isopycnal coordinates with the thickness-weighted averaging. The latter method is preferable in the regions of different stratification for it yields local diapycnal mixing estimates varying less with stratification than their Cartesian coordinate counterparts. Results of this study are comparable to the results of the North Atlantic tracer release experiment (NATRE). However, the internal wave-wave interaction models predict reduced mixing from the breaking of internal waves at low latitudes. Thus, the diapycnal diffusivity found in this study is higher than parameterized by the low latitude of the site (4°N–12°N).

**Citation:** Banyte, D., T. Tanhua, M. Visbeck, D. W. R. Wallace, J. Karstensen, G. Krahmann, A. Schneider, L. Stramma, and M. Dengler (2012), Diapycnal diffusivity at the upper boundary of the tropical North Atlantic oxygen minimum zone, *J. Geophys. Res.*, *117*, C09016, doi:10.1029/2011JC007762.

## 1. Introduction

[2] Diapycnal fluxes of heat, salt, or other dissolved elements (e.g. nutrients, oxygen) are small in comparison to the contribution from advection and along isopycnal mixing in budgets and mass balances. However, in regions with sluggish lateral circulation, the role of vertical mixing in tracer transport can be significant. Such weak horizontal circulation appears, for instance, in the eastern boundary thermocline of the tropical oceans, so-called "shadow zones" of the subtropical gyres [*Luyten et al.*, 1983]. A recent study by *Brandt et al.* [2010], employing a simple ventilation model, showed that the diapycnal mixing could contribute up to 25% of the total oxygen flux into the oxygen minimum zone located in the tropical northeastern Atlantic thermocline. Therefore, it is important to accurately determine diapycnal diffusivity coefficient in order to quantify its contribution to the ventilation of these "shadow zones" and appropriately represent the vertical transport in ocean models.

[3] Direct measurement of turbulent diapycnal mixing in the open ocean is extremely challenging. Most commonly, it is estimated from microstructure shear and temperature measurements which show instantaneous and locally confined turbulent mixing events [e.g., *Gregg et al.*, 1973; *Osborn*, 1980; *Toole et al.*, 1994; *Schafstall et al.*, 2010]. Diapycnal mixing can be also inferred from measurements of vertical shear at scales of tens of meters using lowered ADCP [e.g., *Kunze et al.*, 2006], or from measurements of strain using Conductivity, Temperature, Depth (CTD) sensor data [e.g., *Kunze et al.*, 2006; *Wu et al.*, 2011]. However, the above mentioned methods rely on the parameterizations relating internal wave characteristics and dissipation rates, or diapycnal diffusivity, and hence, are subject to approximations [*Gregg et al.*, 2003; *Kunze et al.*, 2006]. The resulting uncertainty of such estimates is at least of a factor of two [*Polzin et al.*, 1995]. However, since turbulent dissipation typically varies over several orders of magnitude in time and space, those derived methods are invaluable in establishing the local variation in diapycnal diffusivity in the ocean.

[4] A more accurate method to estimate the time-averaged diapycnal mixing is the use of tracer release experiments, where a tracer is released on an isopycnal surface and the diapycnal spread of the tracer is documented with time. The vertical tracer expansion includes all different processes contributing to turbulent mixing and yields a diffusivity estimate integrated over long timescales and large space

[1]GEOMAR, Helmholtz Centre for Ocean Research, Kiel, Germany.
[2]Ocean Science and Technology Oceanography Department, Dalhousie University, Halifax, Nova Scotia, Canada.

Corresponding author: D. Banyte, GEOMAR, Helmholtz Centre for Ocean Research, Duesternbrooker Weg 20, DE-24105 Kiel, Germany. (dbanyte@geomar.de)


0148-0227/12/2011JC007762

**Table 1.** Details of the Three Tracer Sampling Surveys[a]

| Survey | $\Delta T_s$ | Survey Name | Date | Casts (All) | Casts (Tracer) |
|---|---|---|---|---|---|
| Injection | — | MSM08/1 | Apr 23–Apr 26, 2008 | — | — |
| I | 7 months | MSM10/1 | Oct 31–Dec 06, 2008 | 223 | 107 |
| II | 20 months | M80/2 | Nov 28–Dec 22, 2009 | 94 | 80 |
| III | 30 months | M83/1 | Oct 14–Nov 13, 2010 | 72 | 72 |

[a]The second column states the time after tracer injection. The last two columns state the number of CTD casts taken and on how many of these the tracer was found.

scales. Despite the simple concept, the technological challenges of the tracer release experiments are significant, such as the accurate injection of the tracer, detection of the tracer concentrations months after the injection in the long-term experiments, or large sampling area coverage [*Watson and Ledwell*, 2000].

[5] The first large scale tracer release experiment in the open ocean was performed in May 1992. The experiment was led by Ledwell and Watson in the southeastern part of the subtropical gyre, in the region of 20°N–26°N and 30°W–45°W, and was called the North Atlantic Tracer Release Experiment (NATRE) [*Ledwell et al.*, 1993, 1998]. About 140 kg of the tracer, sulfur hexafluoride ($SF_6$), was released on an isopycnal surface near 300 m depth and was surveyed over a period of 30 months as it dispersed across and along isopycnal surfaces. During the 30-month time span, the originally 20-km-wide patch had spread 1000 km horizontally and from about 20 m to 150 m vertically, yielding a vertical diffusivity estimate of $(1.7 \pm 0.2) \times 10^{-5}$ m$^2$ s$^{-1}$.

[6] NATRE results confirmed the estimates obtained from microstructure or fine-scale shear and strain measurements that turbulent diffusivity in the midlatitude thermocline is of the order of $10^{-5}$ m$^2$ s$^{-1}$ [*Gregg*, 1987; *Kunze and Sanford*, 1996; *Kunze et al.*, 2006]. One to two orders of magnitude larger diapycnal diffusivities have been found near boundaries, especially near rough topography [e.g., *Kunze and Sanford*, 1996; *Munk and Wunsch*, 1998; *St. Laurent and Thurnherr*, 2007]. Topographical enhancement of diapycnal mixing was also confirmed by the second large-scale tracer release experiment in the abyssal Brazil basin (BBTRE) on the western flank of the Mid-Atlantic Ridge [*Ledwell et al.*, 2000; *Polzin et al.*, 1997]. Furthermore, several studies show that diapycnal diffusivity varies with latitude and that diffusivity near the equator is less than 10% of that at midlatitudes for a similar background of internal waves [*Henyey et al.*, 1986; *Gregg et al.*, 2003; *Kunze et al.*, 2006].

[7] This study reports on the diapycnal diffusivity estimate from the Guinea Upwelling Tracer Release Experiment (GUTRE) which contributes to the knowledge of mixing processes at low latitudes (4°N–12°N). In the Guinea upwelling region, elevated biological productivity at the surface and weak mean circulation create a low oxygen environment at about 400 m depth and a density level of $\sigma_\Theta = 27.1$ kg m$^{-3}$. The oxygen levels there drop to as low as 40 $\mu$mol kg$^{-1}$ [*Stramma et al.*, 2009], compared to a surface oxygen concentration of about 200 $\mu$mol kg$^{-1}$. The accurate estimate of the diapycnal oxygen supply to the oxygen minimum zone requires the accurate diapycnal mixing estimate, where the vertical oxygen gradient is the largest. Hence, tracer was injected at the upper boundary of the absolute oxygen minimum. 92 kg of the tracer were released on April 2008 at 8°N, 23°W on a density surface $\sigma_\Theta$ = 26.88 kg m$^{-3}$ with a mean depth of 330 m. Three tracer sampling surveys followed (Table 1).

[8] Section 2 describes the experimental setup of GUTRE. Section 3 discusses the experimental strategy and the associated data analysis methods. In particular, the advantage of estimating vertical exchange rates in density coordinates is discussed. Section 4 presents the results from the three tracer surveys and their analysis. Finally, section 5 briefly discusses the main results.

## 2. Experimental Setup

### 2.1. The Site: Guinea Upwelling Region

[9] The study region (Figure 1) is located in the eastern "shadow zone" of the subtropical gyre where the thermocline is ventilated by zonally aligned alternating eastward and westward current branches. The most pronounced eastward flowing current branches transport oxygen-rich waters [*Brandt et al.*, 2008; *Stramma et al.*, 2005]: the North Equatorial Undercurrent (NEUC) and the northern branch of the North Equatorial Countercurrent (nNECC), located at about 5°N and 9°N [*Stramma et al.*, 2005], respectively. On

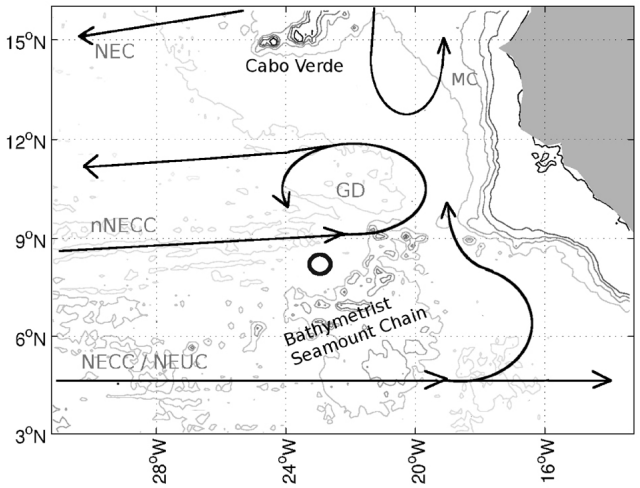


**Figure 1.** Map of the study area, where contours outline the bathymetry above 6000 m depth (contour interval 1000 m). Solid lines mark the schematics of large scale flow field in the thermocline [after *Stramma et al.*, 2008]. Shown are the North Equatorial Current (NEC), the Mauritania Current (MC), the North Equatorial Countercurrent (NECC) connected to the North Equatorial Undercurrent (NEUC), the northern NECC (nNECC) as well as the Guinea Dome (GD). The circle at 8°N, 23°W marks the tracer injection position.

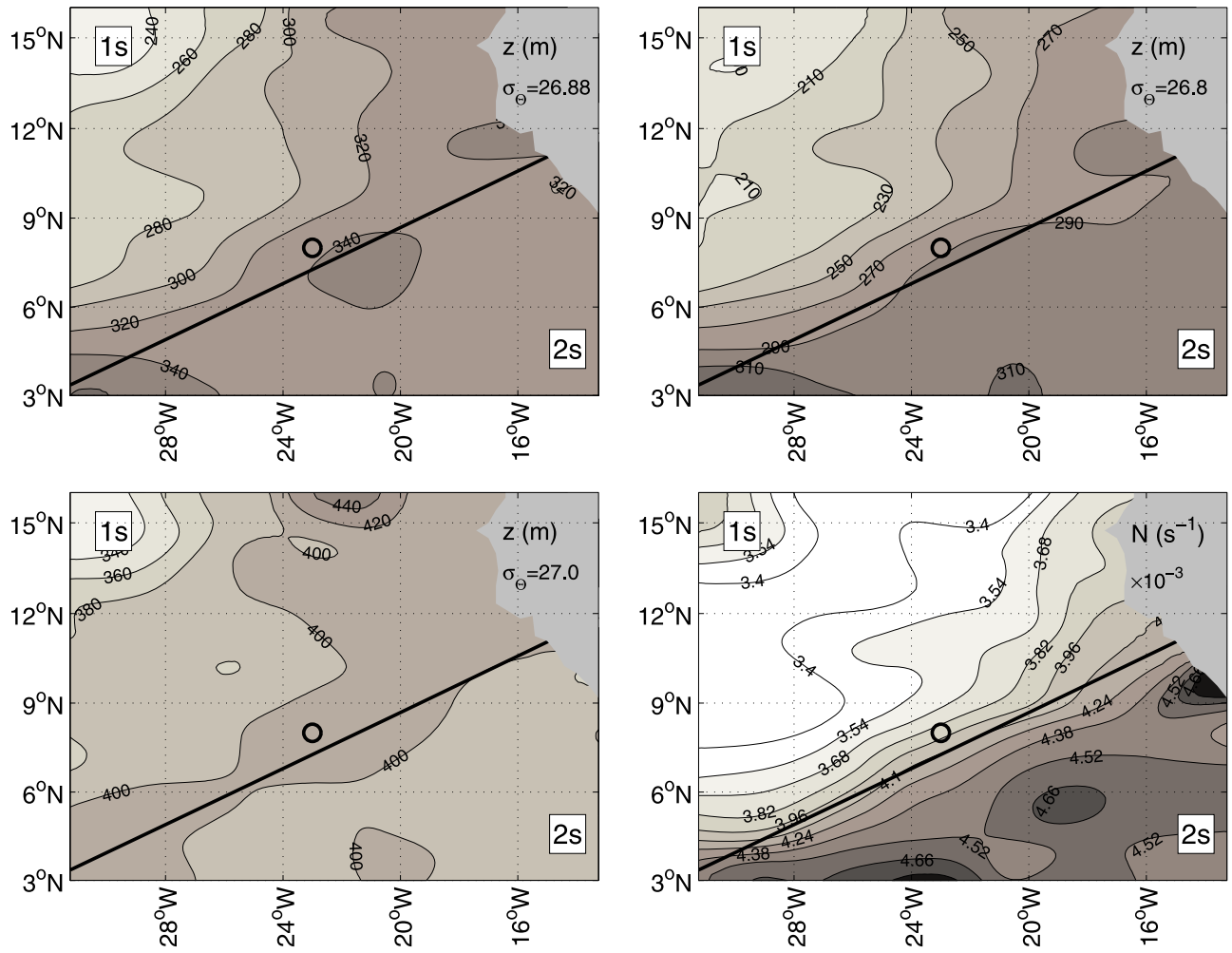


**Figure 2.** Depth of isopycnals $\sigma_\Theta = 26.88$ kg m$^{-3}$, $\sigma_\Theta = 26.8$ kg m$^{-3}$, $\sigma_\Theta = 27.0$ kg m$^{-3}$ and strength of stratification ($N$), where $N$ is the buoyancy frequency. Here $N$ was computed as $N^2 = (g/1026.88)(0.2/(z_{27.0} - z_{26.8}))$. The line separates low (1s) and high (2s) stratification regions. The circle at 8°N, 23°W marks the tracer injection position. The climatology is calculated using the HydroBase2 database of hydrographic profiles [*Curry et al.*, 2003].

the eastern side of the basin, however, the circulation is weak and the mean flow is not well defined. The tracer injection site, 8°N, 23°W, is located in this region of sluggish circulation. Therefore, the tracer was expected to be confined to the region for the experiment's planned duration of 30 months.

[10] The climatological depths of the tracer target density surface $\sigma_\Theta$ = 26.88 kg m$^{-3}$, as well as shallower ($\sigma_\Theta$ = 26.8 kg m$^{-3}$) and deeper ($\sigma_\Theta$ = 27.0 kg m$^{-3}$) isopycnals, are illustrated in Figure 2. The shallower isopycnals are gradually deepening from northwest to southeast affecting the stratification at the tracer target isopycnal. As diapycnal diffusivity estimates might be affected by stratification, two distinctly different regions of stratification were defined (Figure 2): low stratification region (region 1s), and high stratification region (region 2s).

### 2.2. Tracer Release

[11] The tracer released in GUTRE was the halocarbon trifluoromethyl sulfur pentafluoride ($CF_3SF_5$). In earlier tracer release experiments, e.g. NATRE, sulfur hexafluoride ($SF_6$) was used, but recently its use as a purposeful tracer has been discouraged due to its significant and growing global background concentration and use as a transient tracer of ocean ventilation [e.g., *Law and Watson*, 2001; *Tanhua et al.*, 2004; *Bullister et al.*, 2006]. $CF_3SF_5$ has similar properties to $SF_6$, such as very low detection limit, relative ease of analysis, and lack of toxicity but it also has no detectable background concentrations in the ocean [*Ho et al.*, 2008]. It was also chosen as the tracer for an experiment in the Baltic Sea [*Holtermann et al.*, 2012] and for the Diapycnal and Isopycnal Mixing Experiment (DIMES): a large scale tracer release experiment in the Southern Ocean at about 1500 m depth [*Ledwell et al.*, 2011].

[12] In GUTRE, $CF_3SF_5$ was released with the Ocean Tracer Injection System (OTIS) developed at Woods Hole Oceanographic Institution [*Ledwell and Watson*, 1991]. In total, 92 kg, or 470 mol, of tracer was injected in a set of five streaks, within a 20 km by 20 km area, between April 23 and 26, 2008, from R/V *Maria S. Merian.* During the injection, OTIS was towed along the target isopycnal $\sigma_\Theta$ = 26.88 kg m$^{-3}$ (Figure 3). A winch control system automatically

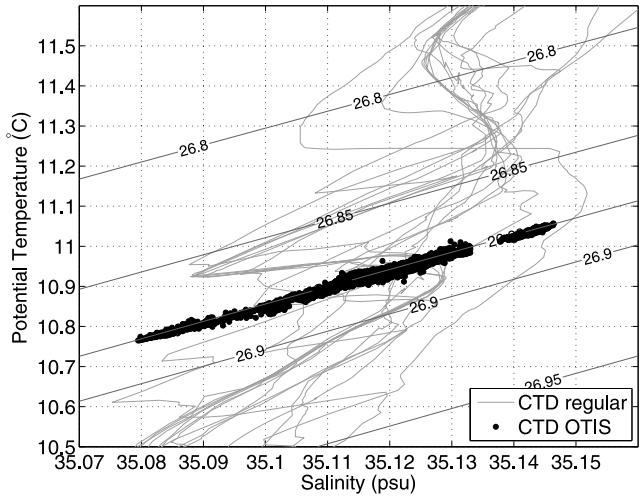


**Figure 3.** TS diagram of water properties during tracer injection at $\sigma_\Theta$ = 26.88 ± 0.005 kg m$^{-3}$ (dots). Regular CTD casts (thin gray lines) were used for calibration of salinity sensors of CTD mounted on OTIS.

responded to the deviation from the target density measured by its built-in CTD (Seabird 911plus CTD). In this way, the root mean square (rms) potential density error in the CTD data for the entire injection was calculated to be only 0.002 kg m$^{-3}$, equivalent to a depth precision of 1.2 m given the mean vertical potential density gradient of 0.0017 kg m$^{-4}$. In addition to the tracer injection uncertainty, turbulent mixing behind the injection sled increased the thickness of the initial tracer layer. During NATRE the initial survey performed 37 hours after tracer injection revealed an initial RMS spread of the tracer of about 2 m [*Ledwell et al.*, 1998]. The RMS potential density error of the tracer injection, as well as the mean vertical potential density gradient and the use of the OTIS system were all similar for GUTRE. Hence, we assumed that the initial RMS width of the tracer injection cloud was 2 m (or 0.0034 kg m$^{-3}$).

[13] During the campaign, two CTD systems were used: one was mounted on OTIS during injection and the other, a regular profiling CTD, recorded water column profiles in between the injections. The regular profiling CTD was calibrated with more than 180 salinity samples taken along the survey and measured on board using a Guildline Autosal 8400B salinometer. The salinometer was regularly calibrated using IAPSO Standard Seawater. The uncertainty of the calibrated temperature was less than 0.002°C and the uncertainty of the calibrated salinity was less than 0.003, resulting in overall absolute density error from the regular CTD of about 0.004 kg m$^{-3}$. It is equivalent to a depth error of 2.5 meters.

[14] OTIS built-in CTD was calibrated to accurately estimate the injection location in density space. The instrument was calibrated by comparison with the calibrated regular CTD data taken in the injection area in between the injections (Figure 3). With the assumption that temperature sensor mounted on OTIS CTD did not require calibration, only conductivity sensor data was compared. The small correction of 0.036 mS cm$^{-1}$ was added to OTIS CTD conductivity sensor data, such that the differences between the temperature data from both instruments were minimized. Taking into account the regular CTD calibration error of 2.5 m and OTIS CTD calibration method, we estimated the absolute depth uncertainty of the tracer injection to about 3 m, equivalent to 0.005 kg m$^{-3}$. Thus, the injection isopycnal was $\sigma_\Theta$ = 26.881 ± 0.005 kg m$^{-3}$.

### 2.3. Tracer Measurements

[15] The tracer ($CF_3SF_5$) samples were taken using a conventional CTD rosette and measured on-board the research vessels within a few hours of sampling. We used three different purge-and-trap gas chromatographic systems equipped with electron capture detectors for the analysis. Two of these systems were slightly modified versions of the set-up described by *Bullister and Weiss* [1988] and *Bullister and Wisegarver* [2008]. Samples were collected in either 100 or 250 mL ground glass syringes from which volumes of 21, 100, or 200 ml, depending on the survey (Table 2), were injected into a purge vessel. For the trap we used a 12 cm long 1/8″ stainless steel (SS) tube packed with Haysep D kept at −30°C during the purge phase. The gases in the trap were desorbed at 120°C onto the pre-column. The third system operated with a vacuum-sparge technique [*Law et al.*, 1994] where the sample was sucked into the purge vessel from an ampule of either 350 or 1400 mL volume. The tracer was trapped within 100 cm of 1/6″ tubing packed with Haysep D and desorbed at 160°C. The chromatographic system was the same: 30 cm 1/8″ SS tube packed with Porasil C kept at 50°–60°C as a pre-column, followed by a 200 cm 1/8″ main-column packed with 180 cm Carbograph 1AC (60–80 mesh) and a 20 cm molecular sieve 5*Å* tail end. The sparging efficiency was continuously checked to ensure 100% (the efficiencies were 93%–96% during the last survey). The sparging times are given in Table 2. This set-up allowed efficient analysis of both $CF_3SF_5$ and dichlorodifluoromethane or CFC-12 (that elutes slightly after, but well separated from, $CF_3SF_5$). Standardization was performed by injecting small volumes of a commercially prepared gaseous standard containing $CF_3SF_5$, but the

**Table 2.** Water Sample Sizes Used to Measure $CF_3SF_5$ During Each Subsequent Survey[a]

| Survey | Period | Sample Volume (ml) | Analyzed Volume (ml) | Precision (fmol kg$^{-1}$) | Detection Limit (fmol kg$^{-1}$) | Sparging Time (min) |
|---|---|---|---|---|---|---|
| I | 7 months | 100 (S) | 21 | 0.9 | 1 | 4 |
| II | 20 months | 250 (S) | 100 | 0.16 | 0.2 | 7 |
| | | 350 (A) | 306 | 0.05 | 0.05 | 20 |
| III | 30 months | 250 (S) | 200 | 0.06 | 0.1 | 10 |
| | | 1400 (A) | 1000 | 0.02 | 0.02 | 20 |

[a]Water samples were collected either with the ground glass syringes (S) or with glass ampules (A). The volume of the analyzed water sample influenced both the precision and detection limit of the measurement.

accuracy of the $CF_3SF_5$ standard is only $\pm 10\%$, and no other reference standards exist today for $CF_3SF_5$. Hence, the absolute values of the measured tracer concentrations were given relative to the biased reference standard, which was the same for all three surveys. However, the absolute value of the $CF_3SF_5$ measurement is not important for the calculations presented in this manuscript.

[16] The precision and detection limit of $CF_3SF_5$ measurements depended on the analyzed seawater volume injected into the purge vessel. Ever decreasing concentrations of the spreading tracer patch, over the course of the 30 month experiment, required ever-larger water volumes to be analyzed (Table 2). During the later surveys, the analyzed seawater volumes varied with depth: larger volumes were used away from the tracer peak isopycnal. The achieved detection limit was about 1 fmol $kg^{-1}$ during the first survey and as low as 0.02 fmol $kg^{-1}$ during the last survey.

## 3. Data Analysis Method

[17] The released tracer dispersed with time along and across isopycnals. In GUTRE, three tracer sampling surveys followed the release.

### 3.1. Averaging Vertical Tracer Profiles

[18] For each survey, a mean tracer profile was constructed similar to *Ledwell et al.* [1998]: (1) the tracer concentration measurements in each cast were 'cubic spline' interpolated over depth onto a one meter bin; (2) density values on one meter intervals were extracted from CTD profile data and binned; (3) alternatively, tracer concentrations were thickness-weighted in each density bin; (4) finally, all individual profiles were interpolated on the same density bin and averaged. The third step, thickness-weighting, is performed to prepare the profiles for the isopynal analysis as described later. In detail, the thickness of each individual profile and each density bin was computed from the density-depth relation smoothed over 0.1 kg $m^{-3}$ density steps. Then the thickness was multiplied by the mean tracer concentration in the density bin to yield tracer (thickness-concentration)-density profile.

[19] The uncertainty ranges of the mean profile were calculated differently from *Ledwell et al.* [1998]. Instead of computing the variance in the shapes of the individual profiles, we used a Monte Carlo method. In detail, the average was calculated for 1000 subsets, each of them consisting of a randomly selected sample of 50% of the vertical tracer profiles from the survey. The 50% range is chosen to represent uncertainty of the bootstrap procedure, where the synthetic data set is generated randomly sampling with replacement. Two standard deviations were taken for the 95% confidence interval of the mean tracer profile. The uncertainty takes into account the variability in the shapes of individual profiles.

### 3.2. Advection-Diffusion Equation in Cartesian Coordinates

[20] The mean tracer spread across isopycnals can be described by the advection-diffusion equation in Cartesian coordinates as

$$\frac{\partial \bar{c}}{\partial t} + w^z \frac{\partial \bar{c}}{\partial z} = \frac{\partial}{\partial z}\left(D^z \frac{\partial \bar{c}}{\partial z}\right), \tag{1}$$

where $D^z$ is the diapycnal diffusion coefficient of the tracer, $w^z$ is vertical velocity, and $\bar{c}$ represents the regional average of the tracer concentration. In this study, we also used the expanded version of equation (1), as adopted from *Ledwell et al.* [1998, equation (7)]:

$$\frac{\partial \bar{c}}{\partial t} + \left(w^z - \frac{\partial D^z}{\partial z}\right)\frac{\partial \bar{c}}{\partial z} = D^z \frac{\partial^2 \bar{c}}{\partial z^2}. \tag{2}$$

The quantity $((\partial z/\partial t)^\sigma)$, which represents the vertical movement of isopycnal surfaces relative to the target density surface from survey to survey, was omitted in equation (1). In GUTRE, a large spatial variation in stratification (Figure 2) did not allow to observe its temporal changes.

[21] When tracer spreads in the field, where stratification regionally varies, the equation in Cartesian coordinates must, however, be used with care. In special situations, the tracer analysis in Cartesian coordinates may lead to the paradox of negative diapycnal diffusion rates. As a thought experiment, lets assume that the evolving tracer patch is advected over time from low to high stratification regions. In density space, the mean tracer thickness is always increasing with time, but in Cartesian space, thickness is decreasing due to compression of the isopycnals, which leads to the negative $D^z$ estimate.

### 3.3. Advection-Diffusion Equation in Isopycnal Coordinates

[22] It is helpful to apply advection-diffusion equation written directly in isopycnal coordinates. Especially, when tracer profiles are initially averaged over density to avoid the effect of transient isopycnal displacements due to internal waves and other oceanic variability. Following *de Szoeke and Bennett* [1993], the advection-diffusion equation in isopycnal coordinates is written as:

$$z_\rho\left(\frac{\partial \bar{c}}{\partial t} + w^\rho \frac{\partial \bar{c}}{\partial \rho}\right) = \frac{\partial}{\partial \rho}\left(D^z \frac{1}{z_\rho}\frac{\partial \bar{c}}{\partial \rho}\right), \tag{3}$$

where $z_\rho = \partial z/\partial \rho$ is the spacing of isopycnals per unit density and is often termed the "thickness"; $w^\rho$ is the diapycnal velocity, which is the difference between vertical velocity $w^z$ and the vertical motion of an isopycnal surface. Note, that the units of $w^\rho$ are kg $m^{-3}$ $s^{-1}$, which when multiplied by the "thickness", $z_\rho$, converts to Cartesian units of m $s^{-1}$.

[23] Before equation (3) is applied to the regionally averaged tracer profiles, the method of averaging becomes important. Commonly, the individual tracer profiles are averaged over isopycnals resulting in a mean tracer concentration-density profile. *De Szoeke and Bennett* [1993] discusses thickness-weighted average for the macroscales, which can be written as $\langle c\rangle = \overline{z_\rho c}/\overline{z_\rho}$. The quantity $\overline{z_\rho c}$ defines the mass of $c$ in the isopycnic volume, i.e., volume between isopycnals of thickness $z_\rho$ and a unit area. Hence, $z_\rho c$ assures that with varying isopycnal thickness from one region to the other, volumetric concentration of $c$ stays the same.

[24] The advection-diffusion equation in isopycnal coordinates with thickness-weighted average is written as:

$$\overline{z_\rho}\left(\frac{\partial \langle c\rangle}{\partial t} + \langle w^\rho\rangle \frac{\partial \langle c\rangle}{\partial \rho}\right) = \frac{\partial}{\partial \rho}\left(D^z \frac{1}{\overline{z_\rho}}\frac{\partial \langle c\rangle}{\partial \rho}\right), \tag{4}$$

where the diapycnal diffusion coefficient is parameterized as [*Osborn and Cox*, 1972; *de Szoeke and Bennett*, 1993]: $D^z = \kappa^\rho \cdot \langle\overline{|\partial\rho_*|^2}\rangle\overline{z_\rho}^2$, where $\kappa^\rho$ is molecular diffusivity of density, considered to be a constant, and $\overline{|\partial\rho_*|^2}$ is the mean square density variance. Introducing a new quantity $D^\rho = \kappa^\rho \cdot \overline{|\partial\rho_*|^2}$, the diapycnal diffusion coefficient $D^z$ in equation (4) can be rewritten as $D^z = \langle D^\rho\rangle\ \overline{z_\rho}^2$. Expanding all of the thickness-weighted averaging operators gives:

$$\left(\frac{\partial\overline{z_\rho c}}{\partial t} + \frac{\overline{z_\rho w^\rho}}{\overline{z_\rho}}\frac{\partial\overline{z_\rho c}}{\partial\rho}\right) = \frac{\partial}{\partial\rho}\left(\frac{\overline{z_\rho D^\rho}}{\overline{z_o}}\frac{\partial\overline{z_\rho c}}{\partial\rho}\right), \tag{5}$$

or

$$\left(\frac{\partial\overline{z_\rho c}}{\partial t} + \langle w^\rho\rangle\frac{\partial\overline{z_\rho c}}{\partial\rho}\right) = \frac{\partial}{\partial\rho}\left(\langle D^\rho\rangle\frac{\partial\overline{z_\rho c}}{\partial\rho}\right). \tag{6}$$

[25] Advection-diffusion equations written in terms of Cartesian coordinates (equation (1)) and isopycnic coordinates (equation (6)) are comparable when $w^z$ is exchanged with $\langle w^\rho\rangle$, $D^z$ with $\langle D^\rho\rangle$, and $\bar{c}$ is exchanged with $\overline{z_\rho c}$. The units of all the quantities in equation (6) are all isopycnic: $\langle w^\rho\rangle$ has units of kg m$^{-3}$ s$^{-1}$, $\langle D^\rho\rangle$ has units of (kg m$^{-3}$)$^2$ s$^{-1}$, and $\overline{z_\rho c}$ units of mol m kg$^{-1}$. From here on we omit the averaging brackets for the simplicity, bearing in mind that all isopycnal analysis is done with the applied thickness-weighted average.

[26] The newly defined $D^\rho$ has a meaning of diapycnal diffusion coefficient expressed in isopycnic units. In literature, various symbols are used to indicate the diapycnal diffusion coefficient expressed in Cartesian units, most commonly: $K_z$, $K_\rho$, $D_z$. In this study, we use the superscript instead of the subscript to mark the choice of coordinate system to distinguish it from the notation of the derivative. Thus, $D^z$ refers to Cartesian units of m$^2$ s$^{-1}$ and $D^\rho$ to isopycnic units of (kg m$^{-3}$)$^2$ s$^{-1}$.

### 3.4. Discretization of Advection-diffusion Equation

[27] Equations (1) and (6) are identical in the form and can be expanded the same way as equation (2). The same discretization algorithm was applied for both equations. Equation (2) was discretized using a forward-time, centered-space algorithm as in [*Glover et al.*, 2011]:

$$c_i^{n+1} = a_- c_{i-1}^n + a_0 c_i^n + a_+ c_{i+1}^n, \tag{7}$$

where $a_- = b/2 + d$, $a_0 = 1 - 2d$, and $a_+ = -b/2 + d$, defining a dimensionless advection number as $b = [(w^z - \partial D^z/\partial z)\Delta t]/\Delta z$, and a dimensionless diffusion number as $d = [(D^z + z \times (\partial D^z/\partial z) + z_0)\Delta t]/(\Delta z)^2$. Here $z$ is the vertical coordinate and $z_0$ - its first (and lowest) value. Thus, positive $\partial D^z/\partial z$ indicates a diapycnal diffusivity that decreased with increasing depth.

[28] The numerical solution of the advection-diffusion equation with three adjustable parameters: $D^z$, $\partial D^z/\partial z$, and $w^z$, was fitted to the mean vertical tracer profile of each survey. The equation used an initial Gaussian tracer distribution with a second moment of 2 m, or 0.0034 kg m$^{-3}$ (the precision of the tracer injection). The optimal set of adjustable parameters was found by maximum likelihood estimate, which minimized $\chi^2$ defined as:

$$\chi^2 = \sum_i [(c_i' - \bar{c}_i)/\delta_i]^2 \tag{8}$$

where the prime indicates model results, $\bar{c}$ the observations, and $\delta$ the observational uncertainty of the vertical tracer profile.

[29] The uncertainty of the vertical mixing parameters was evaluated using the Monte Carlo method. In detail, the maximum likelihood estimate ($\chi^2$) and corresponding numerical best-fit solution were computed with a generated set of 1000 mean vertical tracer profiles for each survey. Each profile in a set was averaged over the 50% randomly selected profiles in a survey. Two standard deviations in parameters $D^z$, $\partial D^z/\partial z$, and $w^z$ defined the 95% confidence interval.

### 3.5. Gaussian Fit Approach

[30] When the mean vertical tracer profiles closely resemble Gaussian shapes, the simple diffusion model fully describes the vertical widening of a tracer. Then, the diapycnal diffusion coefficients ($D^z$ and $D^\rho$) can be directly estimated from the time series of the second moments, while the diapycnal velocities ($w^z$ and $w^\rho$) can be calculated from the corresponding first moments. The Gaussian fit was applied both to the mean tracer concentration-density and (thickness-concentration)-density profiles. In the first case, the estimated parameters had Cartesian units ($D^z$ and $w^z$) and in the second case - isopycnic units ($D^\rho$ and $w^\rho$).

[31] The uncertainties of the diapycnal diffusion coefficient and the diapycnal velocity were computed following a similar procedure as above. In detail, the Gaussian was fitted and, thus, $D^z$ and $w^z$ calculated, for each averaged vertical tracer profile of 1000 subsets. Two standard deviations in $D^z$ and $w^z$ variation were set for the 95% confidence interval.

## 4. Results

[32] The three major tracer surveys followed 7, 20, and 30 months after the injection. The individual tracer profiles in each survey were averaged over density to obtain the mean tracer concentration-density or mean tracer (thickness-concentration)-density profile. Then, for the Cartesian coordinate analysis, the density coordinate was transformed to the height coordinate using the mean density-depth relation. Finally, the diapycnal mixing parameters were estimated by solving advection-diffusion equations both in Cartesian and in isopycnal coordinates.

### 4.1. Spreading of the Tracer

[33] The first survey after tracer injection was performed in November 2008 (after 7 months) from R/V *Maria S. Merian* (Table 1). The biggest challenge was to capture the narrow streaks of the spreading tracer patch. The tracer concentrations between the casts varied significantly, even when separated by distances as small as 30 km (Figures 4a and 4b). In total, the tracer was detectable in about 50% of the casts (Table 1) and most of it was found in the region 20°W–24°W, 6°N–11°N.

[34] The second survey followed in December 2009 (after 20 months) from R/V *Meteor*. In the sampled region of 4°N–14°N, 15°W–30°W (Figure 4c), the tracer was detected in about 85% of all casts. The third survey was performed in October–November 2010 (after 30 months) from R/V *Meteor* in the region of 3°N–15°N, 15°W–28°W (Figure 4d). Here, the tracer was detected in all of the casts and the tracer inventory

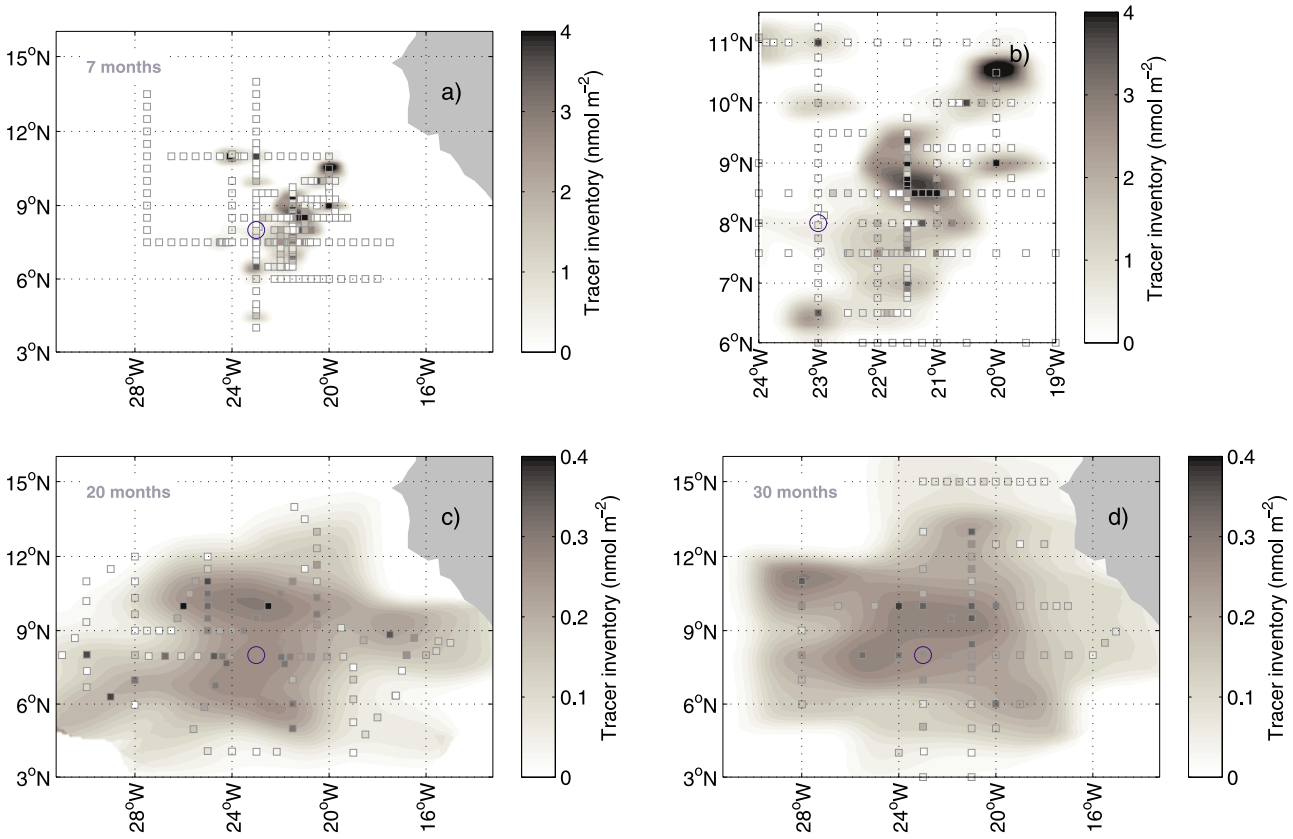


**Figure 4.** Horizontal tracer patch distribution during three surveys: (a and b) in November 2008 (7 months after tracer release), (c) in December 2009 (20 months after tracer release), and (d) in October–November 2010 (30 months after tracer release). The color of the squares represents the tracer column integral; the same color bar applies to the filled contours. The blue circle at 8°N, 23°W marks the tracer injection position, but the symbol is larger than the 20 km by 20 km area of the injection.

distribution shows that the tracer patch expanded farther to the west than the westernmost sampled longitude of 28°W.

[35] The contour maps of the tracer column integrals (Figure 4) illustrate the lateral tracer patch distribution for each survey. The contours were interpolated using Gaussian weights, where the meridional radius of influence is chosen arbitrarily to be 25 km (first survey) and 100 km (second and third surveys). The zonal radius of influence was twice as large. Furthermore, the zeros were assigned at a cut-off radius distance from the nearest cast position; cut-off radius being two times the radius of influence. The sum of the smoothed tracer inventories for the first, second, and third surveys roughly indicate that about 50%, 60%, and 70% of all the injected tracer was found, respectively. It is important to note that the uncertainties of such inventory calculations are large and the estimates must be used with care. Overall, the visual inspection of the lateral tracer patch distribution suggests a large amount of tracer clustered near the injection site for all three surveys and implies little mean lateral advection in the region.

[36] The tracer patch expanded vertically from a thickness of about 80 m in seven months to almost 200 m in thirty months after injection. The individual tracer concentrations, as measured in water samples taken from the Niskin bottles, are shown in Figure 5. During the first survey, the maximum tracer concentrations peaked at 230 fmol kg$^{-1}$, but half of the profiles had peak concentrations in the range of 10 to 70 fmol kg$^{-1}$. In the second survey, the peak concentrations dropped significantly: mostly in the range of 2 to 4 fmol kg$^{-1}$, while the largest overall measured concentration reached 6.5 fmol kg$^{-1}$. The third survey, which was carried out ten months later, had largest concentrations of about 4 fmol kg$^{-1}$ and half of the peak concentrations varied in the range of 1 to 2.5 fmol kg$^{-1}$.

[37] Several examples of the individual tracer concentration-height profiles for each subsequent survey are shown in Figures 6, 7, and 8, respectively. The tracer profiles in the first survey mostly had narrow single peaks located at different densities. The mean vertical profile, respectively, had large uncertainty ranges. In the second survey, the vertical tracer profiles were broader and better resolved by imposed minimum sampling distance of 10 m. A bimodal distribution was often found in the vertical tracer profiles resulting in high variability in the shapes of the profiles. In the third survey, the individual vertical tracer profiles started to resemble Gaussian distribution with fewer low concentration intrusions.

[38] In summary, the spatial and vertical distribution of the tracer patch found in three surveys agrees with the previously suggested image of how the tracer evolves with time [*Ledwell et al.*, 1998]. In the beginning, the tracer patch is comprised of a number of streaks as narrow as tens of


**Figure 5.** Tracer concentrations sampled at discrete depth levels for three surveys: 7, 20, and 30 months after the tracer injection. The detection limits of the surveys were 1 fmol kg$^{-1}$, 0.05–0.2 fmol kg$^{-1}$, and 0.02–0.1 fmol kg$^{-1}$, respectively.

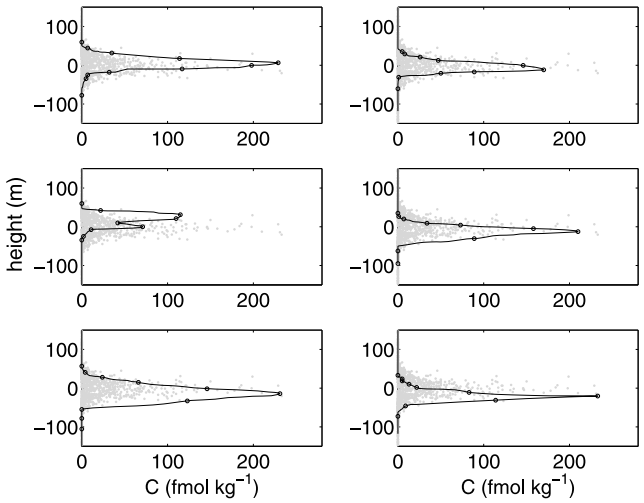


**Figure 6.** Six individual tracer profiles with the largest vertical tracer concentration integral value during the first survey in November 2008 (7 months after tracer release). The ordinate is height above the target density surface in the mean potential density gradient of 0.0017 kg m$^{-4}$. Grey dots in the background mark all of the measured data in the survey.

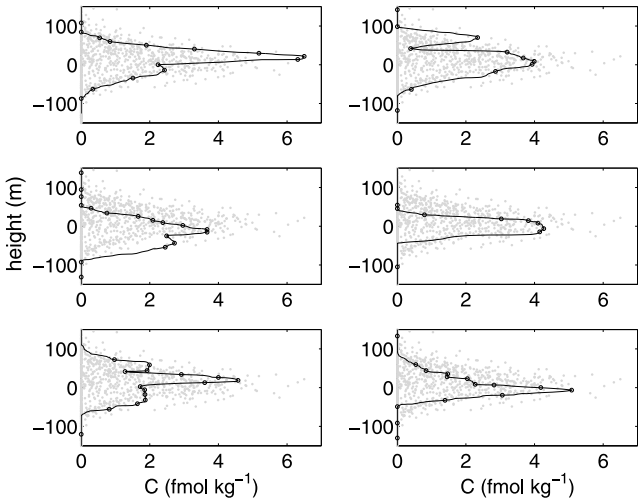


**Figure 7.** Same as in Figure 6, but during the second survey (20 months after tracer release).

kilometers. The vertical tracer profiles are strongly distorted. However, after 30 months the streaks have merged and individual vertical tracer profiles start to resemble a Gaussian distribution. Also the higher tracer column inventories were found near the injection site for each survey, indicating a weak mean advection of the center of mass of the evolved tracer patch. We conclude, that in agreement with the expected weak lateral circulation of the "shadow zone" thermocline, the tracer patch stayed on the eastern side of the basin for the whole period of 30 months and was first streaked, but later homogenized by the lateral eddies.

### 4.2. Density-Depth Relation

[39] The mean density-depth profile enables the conversion of vertical coordinates from density to height above the tracer injection isopycnal. The profile and its error ranges were computed from the data merged from the three tracer surveys and binned in a 1° × 1° grid (Figure 9). Individual profiles revealed a large variation in the depth of the isopycnals above the target density $\sigma_\Theta$ = 26.88 kg m$^{-3}$. This

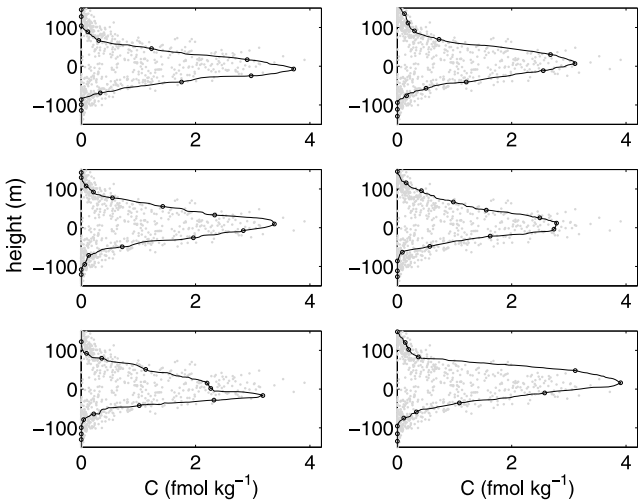


**Figure 8.** Same as in Figure 6, but during the third survey (30 months after tracer release).

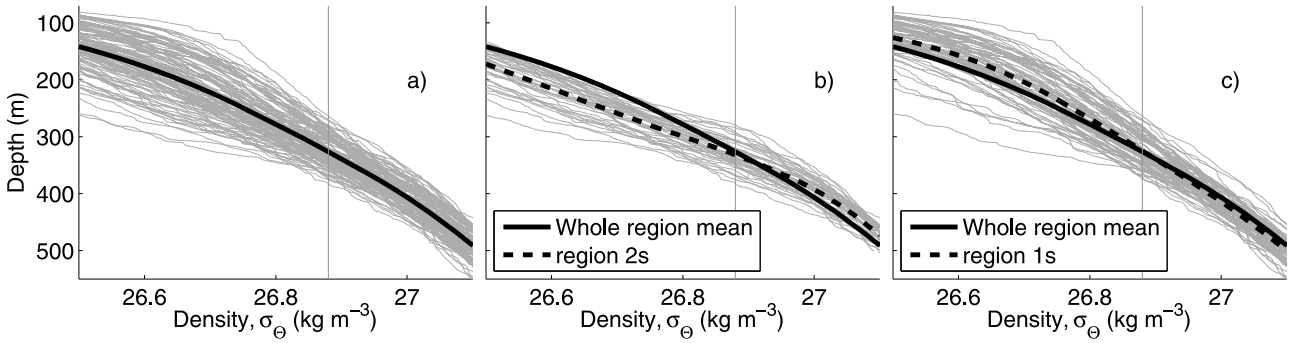


**Figure 9.** Density-depth profiles (thin gray lines) from the three tracer sampling surveys, binned over 1° × 1° grid: (a) over the whole region, (b) in high stratification region (2s), and (c) in low stratification region (1s). The vertical line indicates the isopycnal of the tracer injection. The solid line (same in all three graphs) represents the mean vertical density profile for the whole region. The dashed line represents the local mean vertical density profile.

corresponds to the systematic variability of stratification in the region (Figure 2). To investigate the influence of stratification on our calculations, we separately computed the diapycnal diffusion coefficient in two regions of distinctively different stratification (1s and 2s in Figure 2) using the corresponding local mean density-depth profiles as marked in Figures 9b and 9c.

[40] The mean density gradient was computed in the density range of ±0.05 kg m$^{-3}$ around the tracer target isopycnal both locally and over the whole region. The density gradient in region (1s) was 0.0015 kg m$^{-4}$ resulting in the buoyancy frequency of $N = 3.8 \times 10^{-3}$ s$^{-1}$. Region (2s) had about a 30% larger stratification ($N = 4.7 \times 10^{-3}$ s$^{-1}$) corresponding to the mean density gradient of 0.0023 kg m$^{-4}$. Over the entire region, the mean buoyancy frequency was $N = 4.0 \times 10^{-3}$ s$^{-1}$ with the mean density gradient of 0.0017 kg m$^{-4}$.

### 4.3. Diapycnal Diffusion Coefficient Estimate

[41] The diapycnal diffusion coefficient was estimated by numerically solving advection-diffusion equation (7) or by the Gaussian fit applied to the regionally averaged vertical tracer profiles (Figures 10 and 11). For the Cartesian coordinate analysis tracer concentration-height profiles were used (Figure 12), while for the isopycnal coordinate analysis thickness weighted tracer concentration-density profiles were analyzed (Figure 11).

[42] The mean diapycnal diffusion coefficient estimate from the two methods and over the whole region and the period of 30 months was $D^z = (1.19 \pm 0.18) \times 10^{-5}$ m$^2$ s$^{-1}$, or $D^\rho = (3.07 \pm 0.58) \times 10^{-11}$ (kg m$^{-3}$)$^2$ s$^{-1}$. The result is an average of estimates from the three surveys (Table 3), each computed starting with the time of injection. As expected, $D^z$ and $D^\rho$ estimates from both Gaussian fit approach and numerical solution of the advection-diffusion equation were similar (Figure 13), since the mean vertical tracer profiles closely resembled Gaussian shapes (Figure 12). Between the two coordinate systems in which parameters were estimated, the results differ by only 0.13 m$^2$ s$^{-1}$ and the difference is not significant in the range of uncertainties. $D^\rho$ converted to

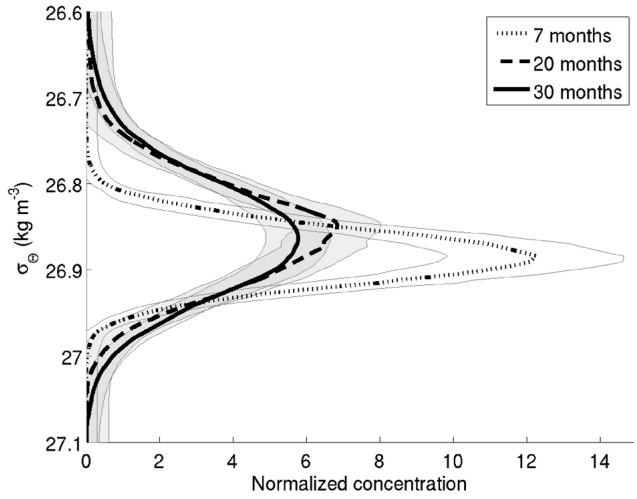


**Figure 10.** Normalized mean vertical tracer profiles for each of the three surveys. Uncertainty represents the variability in the shapes of the individual tracer profiles and the detection limit.

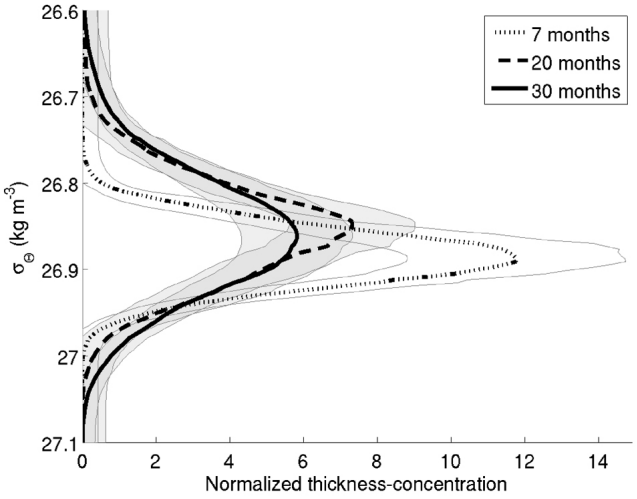


**Figure 11.** Normalized thickness-weighted average tracer profiles for each of the three surveys. Uncertainty represents the variability in the shapes of the individual tracer profiles and the detection limit.

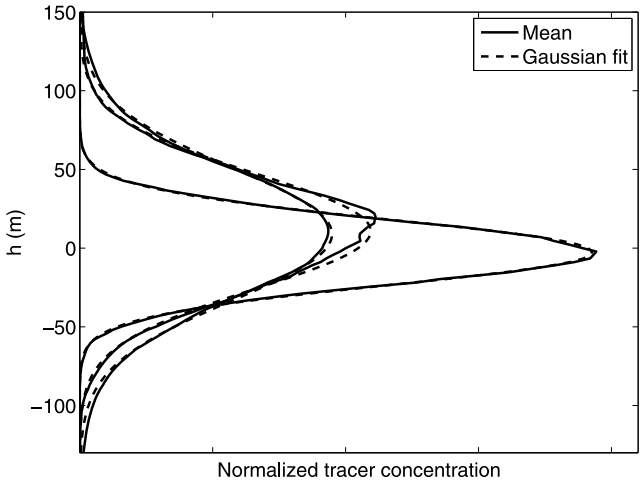


**Figure 12.** Normalized mean vertical tracer profiles for each of the three surveys, as in Figure 10, but ordinate is converted to height above the target density surface using the mean density-depth profile (Figure 9a). The Gaussian distributions fitted to the profiles are marked by the dashed lines.

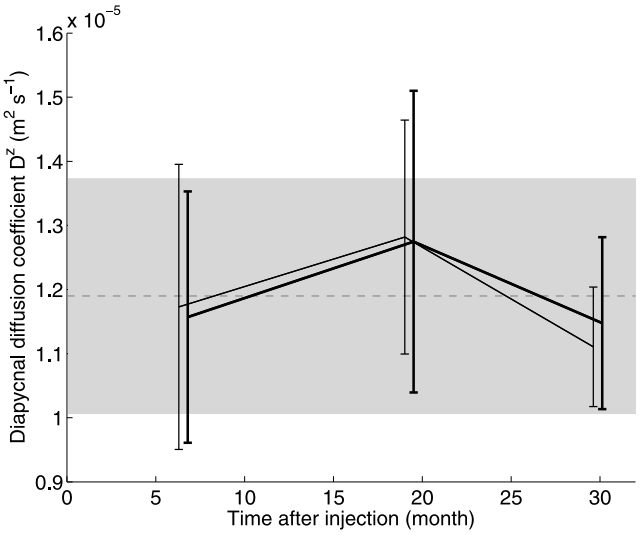


**Figure 13.** Diapycnal diffusivity in Cartesian coordinates for each of the three surveys, computed starting with the initial tracer injection profile. The thin line (shifted in time for better visibility) marks the result from the Gaussian fit method, and the thick line is the numerical solution. The whole region mean (dashed line) and uncertainty ranges (gray patch) are computed using Monte Carlo method, where subsets are randomly picked from the uncertainty ranges of each survey.

Cartesian units using density-depth gradient averaged over the whole region (0.0017 kg m$^{-4}$) results in (1.06 $\pm$ 0.2) $\times$ $10^{-5}$ m$^2$ s$^{-1}$ estimate.

[43] The diapycnal diffusion coefficient estimates differed only slightly from survey to survey given the range of uncertainties. The main source of uncertainty arose from the distortions of the individual vertical tracer profiles, and hence the homogeneity of the tracer patch. However, the time errors due to the duration of the tracer sampling survey and the precision of the tracer injection have also been accounted for. All of the errors decreased significantly with time: the sampling error due to the increasing homogeneity of the tracer patch, the other two errors due to the increasing time interval between the tracer injection and the survey. The survey's sampling time period of about one month increased the diapycnal diffusivity estimate error in the first survey, contributing almost the same as all other error sources together. After 30 months, the error associated with survey's duration accounted for about 20% of the overall error.

### 4.4. Diapycnal Velocity and Diapycnal Diffusivity Gradient

[44] The diapycnal velocity estimate over the period of 30 months was $w^z$ = (0.5 $\pm$ 1.5) $\times$ $10^{-7}$ m s$^{-1}$, or $w^\rho$ = (1.5 $\pm$ 2.7) $\times$ $10^{-10}$ kg m$^{-3}$ s$^{-1}$, but a large variation of estimates from survey to survey was observed (Table 3). During the first survey, the peak of the mean tracer profile was located below the injection density by about 2 m. This resulted in a negative diapycnal velocity estimate of ($-1.5$ $\pm$ 2.6) $\times$ $10^{-7}$ m s$^{-1}$. Deepening of the tracer patch has been observed in previous tracer release experiments [*Ledwell and Watson*, 1991; *Ledwell and Bratkovich*, 1995; *Ledwell et al.*, 1998]. This was attributed either to the sinking of the tracer droplets before dissolving, or to the adsorption of tracer onto the sinking particulates, or salt finger fluxes. In GUTRE, however, the tracer patch was found to have risen during the two later surveys, 20 and 30 months after tracer injection. The tracer peak during both surveys was located about 10 m above the target isopycnal. When calculated over the last two surveys, the mean diapycnal velocity was $w^z$ = (1.5 $\pm$ 1.0) $\times$ $10^{-7}$ m s$^{-1}$ (i.e., approximately 5 m yr$^{-1}$). The vertical gradient of the diapycnal mixing coefficient ($\partial D^z/\partial z$) was analyzed as one of the mechanisms which might explain the observed tracer peak rising through the isopycnals.

[45] The vertical gradient of diapycnal mixing coefficient ($\partial D^z/\partial z$) skews the tracer profiles. A constant positive $\partial D^z/\partial z$ would cause the peak of a Gaussian distribution to migrate downward with velocity $-2\partial D^z/\partial z$, while the center of mass of the distribution would migrate upwards with velocity $\partial D^z/\partial z$, resulting in a distorted profile [*Ledwell et al.*, 1998]. However,

**Table 3.** Diapycnal Diffusivity and Diapycnal Velocity for Each Survey

| Survey | Time (Months) | $D^\rho \times 10^{-11}$ ((kg m$^{-3}$)$^2$ s$^{-1}$) | $w^\rho \times 10^{-10}$ (kg m$^{-3}$ s$^{-1}$) | $D^z \times 10^{-5}$ (m$^2$ s$^{-1}$) | $w^z \times 10^{-5}$ (m s$^{-1}$) |
|---|---|---|---|---|---|
| I | 6.8 | 3.14 $\pm$ 0.68 | $-2.5$ $\pm$ 4.5 | 1.17 $\pm$ 0.21 | $-1.5$ $\pm$ 2.5 |
| II | 19.5 | 3.13 $\pm$ 0.60 | 4.5 $\pm$ 2.0 | 1.28 $\pm$ 0.21 | 2.0 $\pm$ 1.2 |
| III | 30.1 | 2.91 $\pm$ 0.33 | 2.4 $\pm$ 1.2 | 1.13 $\pm$ 0.11 | 1.0 $\pm$ 0.7 |
| | **Average** | **3.07** $\pm$ **0.58** | **1.5** $\pm$ **2.7** | **1.19** $\pm$ **0.18** | **0.5** $\pm$ **1.5** |

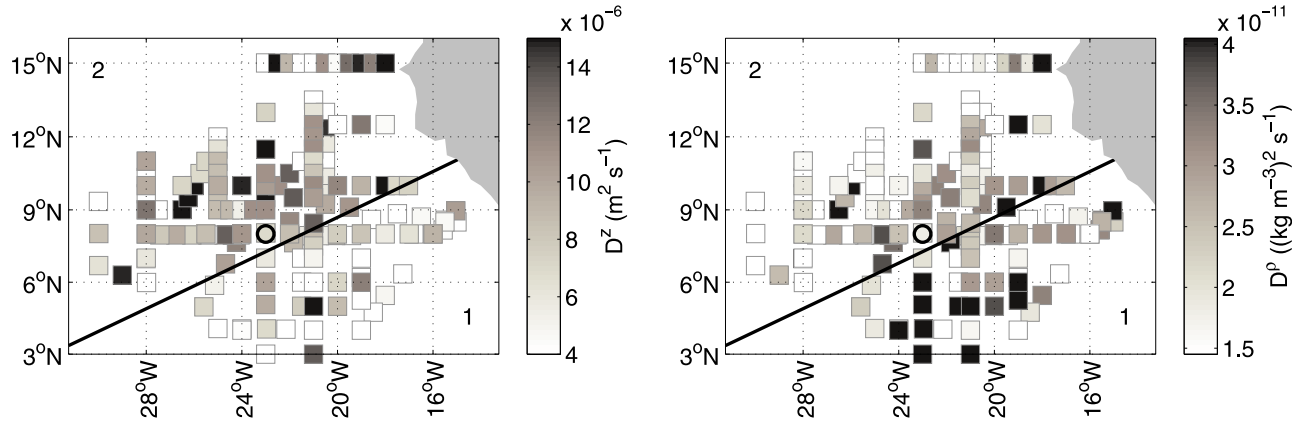


**Figure 14.** Regional variability of the diapycnal diffusion coefficient (left) in Cartesian units and (right) in isopycnic units. The coefficients where computed for each individual vertical tracer profile of the last two surveys. The color bar ranges are adjusted to be comparable using the mean density gradient of 0.0017 kg m$^{-4}$.

the evaluated vertical gradient of the diapycnal diffusion coefficient for all three surveys was nearly zero within the uncertainty range: $(-1.2 \pm 4.9) \times 10^{-8}$ m s$^{-1}$. The negative sign indicates the downward increase of the diapycnal mixing coefficient. The very small estimate of skewness justifies the fitting of a Gaussian distribution model to the data. Consequently, the $\partial D^z/\partial z$ estimate is too small to account for the ascent of the tracer patch through the isopycnals.

### 4.5. Regional Variation of Diapycnal Diffusivity

[46] The thickness of a tracer patch in Cartesian coordinates depends on the local stratification, because an isopycnally homogeneous tracer patch appears thinner in high than in low stratification regions. Thus, differences in the diapycnal mixing estimate derived in Cartesian and in isopycnal coordinates are to be expected between the regions of different stratification. In GUTRE, two distinct regions of different stratification allowed for the comparison of the local $D$ estimates solving the advection-diffusion equation both in Cartesian and in isopycnal coordinates.

[47] A spatial distribution of the thicknesses of the individual tracer profiles was analyzed with respect to the spatial distribution of stratification (Figure 2). The Gaussian distribution was fitted to each individual tracer concentration-depth profile for the Cartesian estimate and to each individual tracer (thickness - concentration) - density profile for the isopycnal estimate. The thickness of each profile was then converted using Fick's law to $D^z$ or $D^\rho$, respectively. The conversion allowed to merge the two last surveys. The data of the first survey was omitted in Figure 14 for simplicity and its limited spatial extent. The color ranges of the maps of $D^z$ (Figure 14, left) and $D^\rho$ (Figure 14, right) were adjusted by using relation: $D^\rho = D^z\overline{\rho_z}^2$, where $\overline{\rho_z}$ is the density gradient averaged over the whole region (0.0017 kg m$^{-4}$). The visual inspection of the diapycnal mixing estimates from the noisy individual profiles indicated that the vertical tracer profiles expressed in meters were found often wider in the low stratification region. $D^\rho$ differences between the regions were less obvious, but a number of large values were found in the high stratification region.

[48] The more stringent analysis of the regional differences between $D^z$ and $D^\rho$ was carried by averaging the tracer profiles in each of the two different stratification regions (denoted 1s and 2s in Figure 2) by the similar procedure as used for the whole region. For Cartesian coordinates, however, the density coordinate was converted to Cartesian coordinate using the regionally averaged density-depth relation (Figures 9b and 9c). In Cartesian coordinates, regional mean $D^z$ estimates were nearly a factor of 2 larger in the low (1s) than in the high (2s) stratification regions, the difference being statistically significant (Table 4 and Figure 15). The analysis carried out in the isopycnal coordinate system, however, yielded a much more similar $D^\rho$ between the two regions. In the low stratification region, the $D^\rho$ estimate was about 25% smaller, but the difference was not significant. In conclusion, instead of reporting two local diapycnal diffusion coefficients ($D^z$) and corresponding mean local stratification, a single $D^\rho$ estimate suffices.

## 5. Discussion

[49] A deliberate tracer release experiment, carried out during the years 2008–2010, was used to study diapycnal

**Table 4.** Local Diapycnal Diffusion Coefficients Averaged Over All Three Surveys[a]

| Region | | $\rho_z$ kg m$^{-4}$ | $D^\rho \times 10^{-11}$ ((kg m$^{-3}$)$^2$ s$^{-1}$) | $D^\rho/\overline{\rho_z}^2 \times 10^{-5}$ (m$^2$ s$^{-1}$) | $D^z \times 10^{-5}$ (m$^2$ s$^{-1}$) |
|---|---|---|---|---|---|
| Low stratification | (1s) | 0.0015 | 2.72 ± 0.68 | 0.94 ± 0.24 | 1.26 ± 0.24 |
| High stratification | (2s) | 0.0023 | 3.48 ± 0.94 | 1.20 ± 0.33 | 0.74 ± 0.15 |

[a] $D^\rho$ was converted to Cartesian units using the whole region's mean density-depth gradient of $\overline{\rho_z}$ = 0.0017 kg m$^{-4}$. $D^z$ was estimated using local mean density-depth relation (as in Figure 9).

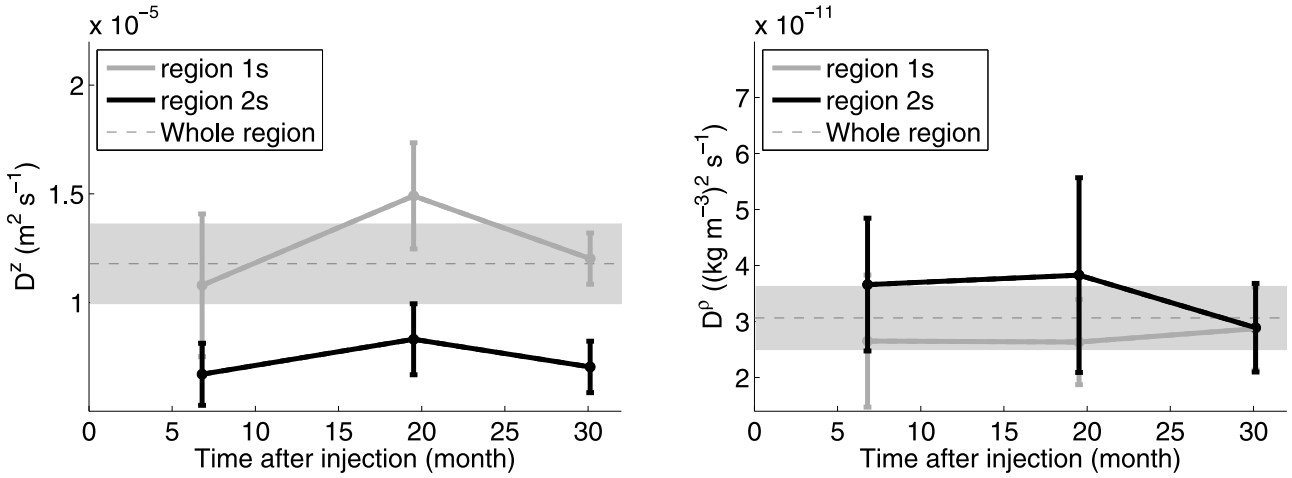


**Figure 15.** Diapycnal diffusivity for each of the three surveys averaged over low (1s) or high (2s) stratification regions. (left) In Cartesian coordinates ($D^z$), computed using the respective local mean density-depth profiles (Figures 9b and 9c). (right) In isopycnal coordinates ($D^\rho$). The gray shading marks the whole region mean estimate of $D^z$ and $D^\rho$, respectively (Table 3).

mixing in the tropical northeastern Atlantic. We have chosen two ways to present the resulting diapycnal mixing estimates: in Cartesian units of $m^2\ s^{-1}$ ($D^z$) and in isopycnic units of $(kg\ m^{-3})^2\ s^{-1}$ ($D^\rho$). $D^\rho$ represents the tracer spreading rate in density coordinates, while $D^z$ is the Cartesian coordinate counterpart. The alternative approach to investigate the tracer spread in isopycnal coordinates follows the method outlined by *de Szoeke and Bennett* [1993] and is motivated by the special stratification conditions; two large permanent regions of distinctive stratification were found in the GUTRE region.

[50] When tracer spreads along isopycnals, it looks thinner in high stratification region, when expressed in Cartesian coordinates. This then translates to a smaller diapycnal mixing coefficient. In GUTRE, the local $D^z$ estimate was nearly a factor of 2 smaller in the high stratification region, while the local $D^\rho$ estimate was more similar between the two regions: ~25% larger and not significant in the range of uncertainties. In general, when a tracer is moving from one region to the other, it is difficult to assess diapycnal diffusion coefficient locally. However, local values of $D$ are needed to calculate the local diapycnal fluxes. One can, similarly, conceive a situation where the tracer distribution was only measured in one of the two density-gradient regions. The diapycnal diffusivity constant in Cartesian coordinates ($D^z$) would then be well determined for this region, but would result in erroneous fluxes if applied to the region with different stratification. The use of the universally determined $D^\rho$ facilitates the local calculations of fluxes, by being less correlated with the local stratification conditions.

[51] The small differences between local $D^\rho$ estimates is a result of the similarity between the thickness-weighted tracer profiles, or the similarity of the diapycnal tracer fluxes in the two regions of different stratification. Considering constant stratification over each of the two regions, differences in the diapycnal tracer flux are expressed through the differences in the diapycnal flux of density ($D^z\overline{\rho_z}$ or $D^\rho/\overline{\rho_z}$). Taking local $D^z$ or $D^\rho$ estimates and corresponding local mean stratification, the local diapycnal density flux differed by less than 20%, which is not significant at the 95% confidence interval. Hence, the diapycnal density flux is a good quantity to compare GUTRE diapycnal mixing results with other tracer release experiments performed under various stratification conditions (Figure 16). The comparison shows that the diapycnal density flux near the rough topography of the Brazil basin (BBTRE [*Polzin et al.*, 1997; *Rye et al.*, 2012]) is similar to the fluxes in the subtropical thermocline (NATRE [*Ledwell et al.*, 1998], GUTRE). They are, however, at least three to four times larger than the fluxes in the high latitude regions of very weak stratification (Greenland Sea [*Watson et al.*, 1999], DIMES [*Ledwell et al.*, 2011]).

[52] In many ways, GUTRE results are comparable to the results of NATRE, performed at a latitude range of 20°N–26°N. Both experiments were carried out at similar depths and had similar mean stratification. GUTRE, however, was

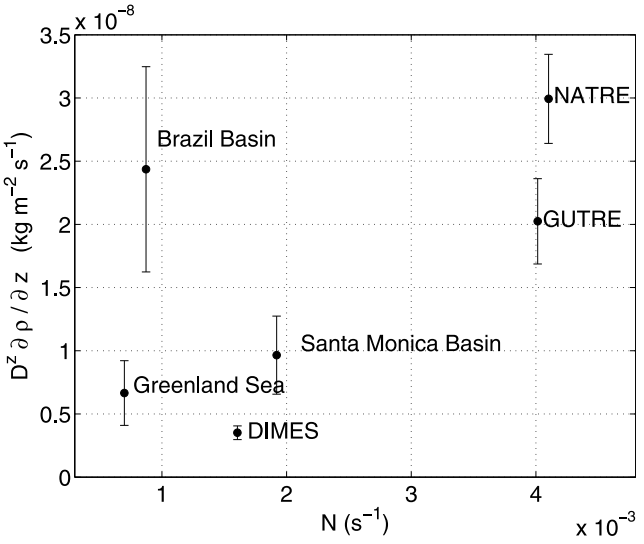


**Figure 16.** Diapycnal flux of density for five earlier tracer release experiments in comparison with the present study (GUTRE) plotted as a function of buoyancy frequency ($N$).

the first tracer release experiment performed in the thermocline at low latitudes (4°N–12°N). Internal wave-wave interaction model [*Henyey et al.*, 1986], recently validated by the observations [*Gregg et al.*, 2003], predicts reduced mixing from the breaking of internal waves at low latitudes. Assuming comparable stratification, internal wave shear levels, and their frequency content at both sites, the diapycnal diffusivity can be parameterized as $K_{pG} = (f_G \cdot \arccos h\,(N_0/f_G))/(f_N \cdot \arccos h\,(N_0/f_N))$ [*Gregg et al.*, 2003; *Kunze et al.*, 2006], where $f_G$ and $f_N$ are Coriolis parameters at the GUTRE and NATRE sites, respectively. In this way, the diapycnal diffusivity at GUTRE site was expected to be smaller by about 60% as compared to the NATRE estimate of $(1.7 \pm 0.2) \times 10^{-5}$ m$^2$ s$^{-1}$. However, the diapycnal diffusivity in GUTRE is only 30% smaller than the estimate of NATRE. This indicates an enlarged background internal wavefield in GUTRE region. Indeed, the hypothesis was confirmed by the accompanying shear microstructure and shipboard ADCP measurements [*Fischer*, 2011].

[53] The larger than expected background internal wavefield found in GUTRE could be evidence of a rough topography effect. The Bathymetrist Seamount Chain located near the tracer release site (Figure 1) has several peaks reaching the depth of the experiment (e.g. Arrayo seamount of 284 m). The presence of rough bottom topography enhances the diapycnal diffusivity by up to one order of magnitude [e.g., *Kunze and Sanford*, 1996; *St. Laurent and Thurnherr*, 2007; *Polzin et al.*, 1997]. Hence, the seamount chain could have acted as a "hot spot" for enhanced diapycnal mixing in GUTRE experiment. However, as the tracer release method is inherently dependent on the entire history of mixing events since the release, the presence of the "hot spot" can only be speculated about.

[54] **Acknowledgments.** We would like to thank all persons involved in the measurement of the tracer as well as the captains, crews and technicians on R/V *Maria S. Merian* and R/V *Meteor* and their home institutions for their support. We thank Jim Ledwell and Richard Greatbatch for the valuable discussions and suggestions. Support for this work came from Deutsche Forschungsgemeinschaft as part of the Sonderforschungsbereich 754 "Climate-Biogeochemistry Interactions in the Tropical Ocean."

## References

Brandt, P., V. Hormann, B. Bourles, J. Fischer, F. A. Schott, L. Stramma, and M. Dengler (2008), Oxygen tongues and zonal currents in the equatorial Atlantic, *J. Geophys. Res.*, *113*, C04012, doi:10.1029/2007JC004435.

Brandt, P., V. Hormann, A. Körtzinger, M. Visbeck, G. Krahmann, and L. Stramma (2010), Changes in the ventilation of the oxygen minimum zone of the tropical North Atlantic, *J. Phys. Oceanogr.*, *40*, 1784–1801.

Bullister, J. L., and R. F. Weiss (1988), Determination of $CCl_3F$ and $CCl_2F_2$ in seawater and air, *Deep Sea Res., Part A*, *35*, 839–853.

Bullister, J. L., and D. P. Wisegarver (2008), The shipboard analysis of trace levels of sulfur hexafluoride, chlorofluorocarbon-11 and chlorofluorocarbon-12 in seawater, *Deep Sea Res., Part I*, *55*, 1063–1074.

Bullister, J. L., D. P. Wisegarver, and R. E. Sonnerup (2006), Sulfur hexafluoride as a transient tracer in the North Pacific Ocean, *Geophys. Res. Lett.*, *33*, L18603, doi:10.1029/2006GL026514.

Curry, R., B. Dickson, and I. Yashayaev (2003), A change in the freshwater balance of the Atlantic Ocean over the past four decades, *Nature*, *426*, 826–829.

de Szoeke, R. A., and A. F. Bennett (1993), Microstructure fluxes across density surfaces, *J. Phys. Oceanogr.*, *23*, 2254–2264.

Fischer, T. (2011), Diapycnal diffusivity and transport of matter in the open ocean estimated from underway acoustic profiling and microstructure profiling, PhD thesis, Dep. of Math. and Nat. Sci., Christian-Albrechts Univ., Kiel, Germany.

Glover, D. M., W. J. Jenkins, and S. C. Doney (2011), *Modeling Methods for Marine Science*, Cambridge Univ. Press, Cambridge, U. K.

Gregg, M. C. (1987), Diapycnal mixing in the thermocline, *J. Geophys. Res.*, *92*, 5249–5289.

Gregg, M. C., C. S. Cox, and P. W. Hacker (1973), Vertical microstructure measurements in the central North Pacific, *J. Phys. Oceanogr.*, *3*, 458–469.

Gregg, M. C., T. B. Sanford, and D. P. Winkel (2003), Reduced mixing from the breaking of internal waves in equatorial waters, *Nature*, *422*, 513–515.

Henyey, F. S., J. Wright, and S. M. Flatte (1986), Energy and action flow through the internal wave field: An eikonal approach, *J. Geophys. Res.*, *91*, 8487–8495.

Ho, D. T., J. R. Ledwell, and W. M. Smethie Jr. (2008), Use of $SF_5CF_3$ for ocean tracer release experiments, *Geophys. Res. Lett.*, *35*, L04602, doi:10.1029/2007GL032799.

Holtermann, P. L., L. Umlauf, T. Tanhua, O. Schmale, G. Rehder, and J. J. Waniek (2012), The Baltic Sea Tracer Release Experiment: 1. Mixing rates, *J. Geophys. Res.*, *117*, C01021, doi:10.1029/2011JC007439.

Kunze, E., and T. B. Sanford (1996), Abyssal mixing: Where it isn't, *J. Phys. Oceanogr.*, *26*, 2286–2296.

Kunze, E., E. Firing, J. M. Hummon, T. K. Chereskin, and A. M. Thurnherr (2006), Global abyssal mixing inferred from lowered ADCP shear and CTD strain profiles, *J. Phys. Oceanogr.*, *36*, 1553–1576.

Law, C. S., and A. J. Watson (2001), Determination of Persian Gulf Water transport and oxygen utilisation rates using $SF_6$ as a novel transient tracer, *Geophys. Res. Lett.*, *28*, 815–818.

Law, C. S., A. J. Watson, and M. I. Liddicoat (1994), Automated vacuum analysis of sulfur hexafluoride in seawater: derivation of the atmospheric trend (1970–1993) and potential as a transient tracer, *Mar. Chem.*, *48*, 57–69.

Ledwell, J. R., and A. Bratkovich (1995), A tracer study of mixing in the Santa Cruz Basin, *J. Geophys. Res.*, *100*, 20,681–20,704.

Ledwell, J. R., and A. J. Watson (1991), The Santa Monica Basin tracer experiment: A study of diapycnal and isopycnal mixing, *J. Geophys. Res.*, *96*, 8695–8718.

Ledwell, J. R., A. J. Watson, and C. S. Law (1993), Evidence for slow mixing across the pycnocline from an open-ocean tracer-release experiment, *Nature 364*, 701–703.

Ledwell, J. R., A. J. Watson, and C. S. Law (1998), Mixing of a tracer in the pycnocline, *J. Geophys. Res.*, *103*, 21,499–21,529.

Ledwell, J. R., E. T. Montgomery, K. L. Polzin, L. C. St. Laurent, R. W. Schmitt, and J. M. Toole (2000), Evidence for enhanced mixing over rough topography in the abyssal ocean, *Nature*, *403*, 179–182.

Ledwell, J. R., L. C. St. Laurent, J. B. Girton, and J. M. Toole (2011), Diapycnal mixing in the Antarctic circumpolar current, *J. Phys. Oceanogr.*, *41*, 241–246.

Luyten, J. R., J. Pedlosky, and H. Stommel (1983), The ventilated thermocline, *J. Phys. Oceanogr.*, *13*, 292–309.

Munk, W., and C. Wunsch (1998), Abyssal recipes II: Energetics of tidal and wind mixing, *Deep Sea. Res., Part I*, *45*, 1977–2010.

Osborn, T. R. (1980), Estimates of the local rate of vertical diffusion from dissipation measurements, *J. Phys. Oceanogr.*, *10*, 83–89.

Osborn, T. R., and C. S. Cox (1972), Oceanic fine structure, *Geophys. Fluid Dyn.*, *3*, 321–345.

Polzin, K. L., J. M. Toole, and R. W. Schmitt (1995), Finescale parameterizations of turbulent dissipation, *J. Phys. Oceanogr.*, *25*, 306–328.

Polzin, K. L., J. M. Toole, J. R. Ledwell, and R. W. Schmitt (1997), Spatial variability of turbulent mixing in the abyssal ocean, *Science*, *276*, 93–96.

Rye, C. D., M. J. Messias, J. R. Ledwell, A. J. Watson, A. Brousseau, and B. A. King (2012), Diapycnal diffusivities from a tracer release experiment in the deep sea, integrated over 13 years, *Geophys. Res. Lett.*, *39*, L04603, doi:10.1029/2011GL050294.

St. Laurent, L. C., and A. M. Thurnherr (2007), Intense mixing of lower thermocline water on the crest of the Mid-Atlantic Ridge, *Nature*, *448*, 680–683.

Schafstall, J., M. Dengler, P. Brandt, and H. Bange (2010), Tidal-induced mixing and diapycnal nutrient fluxes in the Mauritanian upwelling region, *J. Geophys. Res.*, *115*, C10014, doi:10.1029/2009JC005940.

Stramma, L., S. Hüttl, and J. Schafstall (2005), Water masses and currents in the upper tropical Northeast Atlantic off northwest Africa, *J. Geophys. Res.*, *110*, C12006, doi:10.1029/2005JC002939.

Stramma, L., P. Brandt, J. Schafstall, F. Schott, J. Fischer, and A. Körtzinger (2008), Oxygen minimum zone in the North Atlantic south and east of the Cape Verde Islands, *J. Geophys. Res.*, *113*, C04014, doi:10.1029/2007JC004369.

Stramma, L., M. Visbeck, P. Brandt, T. Tanhua, and D. Wallace (2009), Deoxygenation in the oxygen minimum zone of the eastern tropical North Atlantic, *Geophys. Res. Lett.*, *36*, L20607, doi:10.1029/2009GL039593.

Tanhua, T., K. A. Olsson, and E. Fogelqvist (2004), A first study of $SF_6$ as a transient tracer in the Southern Ocean, *Deep Sea. Res., Part II*, *51*, 2683–2699.

Toole, J. M., R. W. Schmitt, and K. L. Polzin (1994), Estimates of diapycnal mixing in the abyssal ocean, *Science*, *264*, 1120–1123.
Watson, A. J., and J. R. Ledwell (2000), Oceanographic tracer release experiments using sulphur hexafluoride, *J. Geophys. Res.*, *105*, 14,325–14,337.
Watson, A. J., et al. (1999), Mixing and convection in the Greenland Sea from a tracer-release experiment, *Nature*, *401*, 902–904.
Wu, L., Z. Jing, S. Riser, and M. Visbeck (2011), Seasonal and spatial variations of Southern Ocean diapycnal mixing from Argo profiling floats, *Nat. Geosci.*, *4*, 363–366.